ISSN 1674-1056
http://cpb.iphy.ac.cn
http://iopscience.iop.org/cpb
中国物理 B
Chinese Physics
中国物理
Chinese Physics B

Direct numerical simulation study on relevance of fluctuating velocities and drag reduction in turbulent channel flow with spanwise space-dependent electromagnetic force

Dai-Wen Jiang(江代文), Hui Zhang(张辉) Bao-Chun Fan(范宝春), An-Hua Wang(王安华)

Citation: Chin. Phys. B . 2019, 28(5): 054701. **doi:** 10.1088/1674-1056/28/5/054701
Journal homepage: http://cpb.iphy.ac.cn; http://iopscience.iop.org/cpb

What follows is a list of articles you may be interested in

Aerodynamic actuation characteristics of radio-frequency discharge plasma and control of supersonic flow

Zhen Yang(杨臻), Hui-Min Song(宋慧敏), Hong-Yu Wang(王宏宇), Shan-Guang Guo(郭善广), Min Jia(贾敏), Kang Wang(王康)
Chin. Phys. B . 2019, 28(2): 024701. **doi:** 10.1088/1674-1056/28/2/024701

A new kind of hairpin-like vortical structure induced by cross-interaction of sinuous streaks in turbulent channel

Jian Li(李健), Gang Dong(董刚), Hui Zhang(张辉), Zhengshou Chen(陈正寿), Zhaode Zhang(张兆德)
Chin. Phys. B . 2018, 27(8): 084701. **doi:** 10.1088/1674-1056/27/8/084701

Mechanism of controlling turbulent channel flow with the effect of spanwise Lorentz force distribution

Yang Han(韩洋), Hui Zhang(张辉), Bao-Chun Fan(范宝春), Jian Li(李健), Dai-Wen Jiang(江代文), Zi-Jie Zhao(赵子杰)
Chin. Phys. B . 2017, 26(8): 084704. **doi:** 10.1088/1674-1056/26/8/084704

Comparison between AlN and Al_2O_3 ceramics applied to barrier dielectric of plasma actuator

Dong-Liang Bian(卞栋梁), Yun Wu(吴云), Min Jia(贾敏), Chang-Bai Long(龙昌柏), Sheng-Bo Jiao(焦胜博)
Chin. Phys. B . 2017, 26(8): 084703. **doi:** 10.1088/1674-1056/26/8/084703

Flow control of micro-ramps on supersonic forward-facing step flow

Qing-Hu Zhang(张庆虎), Tao Zhu(朱涛), Shihe Yi(易仕和), Anping Wu(吴岸平)
Chin. Phys. B . 2016, 25(5): 054701. **doi:** 10.1088/1674-1056/25/5/054701

Direct numerical simulation on relevance of fluctuating velocities and drag reduction in turbulent channel flow with spanwise space-dependent electromagnetic force*

Dai-Wen Jiang(江代文), Hui Zhang(张辉)†, Bao-Chun Fan(范宝春), and An-Hua Wang(王安华)

Science and Technology on Transient Physics Laboratory, Nanjing University of Science and Technology, Nanjing 210094, *China*

(Received 28 November 2018; revised manuscript received 7 January 2019; published online 20 March 2019)

Based on the Fourier–Chebyshev spectral method, the control of turbulent channel flow by space-dependent electromagnetic force and the mechanism of drag reduction are investigated with direct numerical simulation (DNS) methods for different Reynolds numbers. A formula is derived to express the relation between fluctuating velocities and the friction drag coefficient. With the application of electromagnetic force, the in-depth relations among the fluctuating velocities near the wall, Reynolds stress, and the effect of drag reduction for different Reynolds numbers are discussed. The results indicate that the maximum drag reductions can be obtained with an optimal combination of parameters for each case of different Reynolds numbers. The fluctuating velocities along the streamwise and normal directions are suppressed significantly, while the fluctuating velocity along the spanwise direction is enhanced dramatically due to the spanwise electromagnetic force. However, the values of Reynolds stress depend on the fluctuating velocities along the streamwise and normal directions rather than that along the spanwise direction. Therefore, the significant effect of drag reduction is obtained. Moreover, the maximum drag reduction is weakened due to the decay of control effect for fluctuating velocities as the Reynolds number increases.

Keywords: flow control, turbulent channel flow, electromagnetic force, direct numerical simulation

PACS: 47.85.L–, 47.85.lb **DOI:** 10.1088/1674-1056/28/5/054701

1. Introduction

The boundary layer is produced on surfaces of moving objects in the viscous fluid, which leads to deceleration, vibration, and instability. In particular, the friction drag will increase significantly in turbulent flow. Therefore, many control approaches have been used to modify the structures of the boundary layer, which can reduce the friction drag of moving objects. These approaches have a wide prospect of application and great practical value in aviation and navigation.[1–5]

For flow control, the active methods can be distinguished from passive methods by energy input. The electromagnetic control has been considered as one of the most practical active methods due to the flexible design and easy installation.[6] As early as the 1960s, Gailitis found that the boundary layer can be modified by electromagnetic actuators with alternating electrodes and magnets. Subsequently, the control effects of streamwise vortex in turbulence channel flow were investigated numerically by Lim and Choi[7] with electromagnetic force along the streamwise, spanwise, and wall-normal, respectively. The results indicated that the streamwise vortex can be suppressed by both the spanwise and wall-normal electromagnetic force, and the former has more remarkable effects in suppressing streamwise vortices. Jiménez and Pinelli[8] further found that the regenerating cycle mechanism of turbulence depends on the two structures; i.e., quasi-streamwise vortexes and streaks. Next, Satake and Du *et al.*[9–11] studied the turbulent control by electromagnetic force with a spanwise wave traveling along the streamwise direction. They found that the initial near-wall streak structures would replace a wide "ribbon" of low-speed velocity when parameters of electromagnetic force match well, which results in a drag reduction rate up to 30%. Lee *et al.*[12] investigated the vorticity dynamics in the viscous sublayer with the application of electromagnetic force. The results indicated that turbulent structures can be improved near the wall and the skin drag can also be decreased by suppressing the streamwise vortexes of the viscous sublayer. Yin and You[13] studied the characteristics for a cylinder wake with a turbulent boundary layer by using electromagnetic force, and found the force can suppress the flow separation. Moreover, the streamwise traveling and standing waves of velocity imposed at the walls of a plane turbulent channel flow were investigated by Viotti and Quadrio[14,15] with direct numerical simulation (DNS) methods, and the drag reductions were obtained at about 48% and 52% for traveling waves and standing waves, respectively. Moubarak and Habchi[16,17] investigated two scales on the energy cascade in a two-dimension (2D) turbulent flow with electromagnetic force, and found that there exists a linear relationship between the large-scale motion in the atmosphere and the very small ones. Ostillamónico[18] calculated three-

*Project supported by the National Natural Science Foundation of China (Grant No. 11672135) and a Foundation for the Author of National Excellent Doctoral Dissertation of China (Grant No. 201461).

†Corresponding author. E-mail: zhanghui1902@hotmail.com

© 2019 Chinese Physical Society and IOP Publishing Ltd

dimension (3D) turbulent with electromagnetic force by fully solving the Navier–Stokes equations which were coupled with the Poisson–Nernst–Planck equations. The results showed that an ion concentration-dependent viscosity leads to the emergence of a quiescent layer with a higher ion concentration, and the presence of this layer could play a role in disrupting the turbulence generation cycle as one would expect that the turbulence is weaker in regions of higher viscosity, thus potentially decreasing friction. Recently, a DNS study for a fully developed turbulent channel flow was carried out by Altıntaş *et al.*,[19] which introduced a spanwise oscillating electromagnetic force near the lower wall. They observed that the sweeps and ejections moved away from the wall in the fully turbulent region with the application of electromagnetic force. The control effects of streamwise traveling wave and bidirectional wavy electromagnetic force on the wall-turbulence were investigated by our research group.[20,21] The results indicated that the negative streamwise vortex induced by electromagnetic force exists in the flow field with control, which can suppress the inherent positive streamwise vortex and merge the inherent negative streamwise vortex in the turbulent flow field. With the effects of the periodic action, the number of streamwise vortexes and streaks in the flow field was reduced, which further led to the decrease of skin drag.

These studies indicate that the significant effects of turbulence control can be achieved by using electromagnetic force with spanwise oscillating or traveling wave. However, the character structures of the steady flow fields, which depend on the distribution of the electromagnetic force, cannot be obtained due to the time-varying force. With the application of space-dependent electromagnetic force, the regular quasi-streamwise vortex structures in the flow field have been found in our research group. The random velocity fluctuation and mean Reynolds stress can be suppressed by these structures at $Re = 4000$, which further leads to the drag reduction.[22] Therefore, further investigations are necessary on the relations among fluctuating velocities, Reynolds stress, and drag reduction, especially for different Reynolds numbers.

In this paper, the Fourier–Chebyshev spectral method is used to investigate the turbulence channel flow controlled by the space-dependent electromagnetic force using DNS. The spanwise electromagnetic force with sinusoidal distribution along the streamwise direction is selected to control the flow field. Then, the variations of fluctuating velocities, the distributions of Reynolds stress, and the effects of drag reduction of flow field with different Reynolds numbers before and after control are discussed. Moreover, the potential relations among these three are further analyzed by deriving a formula that expresses the relation between the coefficient of friction drag and the fluctuating velocities.

2. Numerical calculations

2.1. Governing equation

Based on the fully developed turbulent flow of a weakly conductive fluid, the flow can be controlled by electromagnetic actuators which are installed on the lower wall of the channel. With the electromagnetic force imposed as a source term, the dimensionless Navier–Stokes equations of incompressible 3D channel flow can be written as

$$\frac{\partial \boldsymbol{u}}{\partial t} + \boldsymbol{u}\cdot\nabla\boldsymbol{u} = -\nabla p + \frac{1}{Re}\nabla^2\boldsymbol{u} + \boldsymbol{f}, \tag{1}$$

$$\nabla\cdot\boldsymbol{u} = 0. \tag{2}$$

Here, all variables are nondimensionalized with respect to the channel half width h and the center line U_c. $\boldsymbol{u}$ is the velocity vector, p is the pressure, $Re = U_c h/\nu$ is the Reynolds number, where ν is the kinematic viscosity coefficient, and $\boldsymbol{f}$ is the electromagnetic force given by

$$\boldsymbol{f} = (0, 0, f_z), \tag{3}$$

where

$$f_z = A\mathrm{e}^{-y/\Delta}\sin\left(\frac{2\pi}{L_x}k_x x\right). \tag{4}$$

Here, f_z is the spanwise electromagnetic force with sinusoidal distributions along the streamwise direction, whose variation depends on space rather than time, A is the non-dimensional amplitude, Δ is the effective penetration of electromagnetic force, and L_x and k_x are respectively the channel length and wave number along the streamwise direction, where $L_x/k_x = \lambda_x$ is the streamwise wave length.

The standard Fourier–Chebyshey spectral method is applied to spatial directions for Eqs. (1) and (2). More details about the numerical methods can be found in Refs. [20]– [22]. The turbulent channel flow is controlled with the application of electromagnetic force at $t = 300$ when the initial disturbance induced for generating a fully developed turbulence has been essentially eliminated, which is steady from $t = 500$ to $t = 1000$. The cases are selected with different Reynolds numbers $Re = 4000$, 5000, 6000, and 7000, corresponding to different viscous lengthscales $\delta_v = 5.54\times10^{-3}$, 4.57×10^{-3}, 3.93×10^{-3}, and 3.44×10^{-3}, respectively.

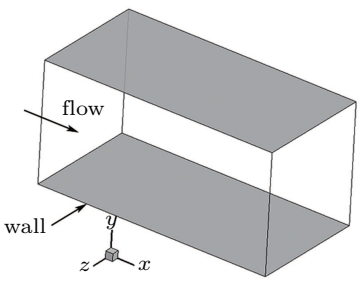


Fig. 1. The schematic diagram of the computational domain.

2.2. Friction drag in turbulent channel flow

Using the Reynolds decomposition in Eq. (1) along the x direction with the streamwise velocity distribution of base flow $U(y) = 1-(1-y)^2 = 2y-y^2$, one obtains

$$\begin{aligned}&\frac{\partial u}{\partial t}+\frac{\partial uu}{\partial x}+\frac{\partial uv}{\partial y}+\frac{\partial uw}{\partial z}\\&=-\frac{\partial p}{\partial x}+\frac{1}{Re}\left(\frac{\partial^2 u}{\partial x^2}+\frac{\partial^2 u}{\partial y^2}+\frac{\partial^2 u}{\partial z^2}\right),\end{aligned}\tag{5}$$

where $u = U(y)+u'$, $v = v'$, $w = w'$, and $p = x\Pi(t)+p'$. Here, y is the distance from the lower wall, u, v, and w are the velocities along the x, y, and z directions, respectively. The superscript $'$ indicates the fluctuation. $\Pi(t)$ is the real-time adjustment of pressure to keep the flow stable.

Then, we have

$$\begin{aligned}&\frac{\partial(U+u')}{\partial t}+\frac{\partial(U+u')(U+u')}{\partial x}\\&+\frac{\partial(U+u')v}{\partial y}+\frac{\partial(U+u')w}{\partial z}\\&=-\Pi(t)-\frac{\partial p'}{\partial x}+\frac{1}{Re}\left[\frac{\partial^2(U+u')}{\partial x^2}\right.\\&\left.+\frac{\partial^2(U+u')}{\partial y^2}+\frac{\partial^2(U+u')}{\partial z^2}\right].\end{aligned}\tag{6}$$

Based on the assumption of the periodic flow structures in the homogeneous directions[23] and the no-slip boundary conditions, which are the basic characters of the turbulent wall-bounded flow, we average Eq. (6) by integrating the equation in the x and z directions, and we have

$$\frac{\partial\overline{u'}}{\partial t}+\frac{\partial\overline{uv}}{\partial y}=-\Pi(t)+\frac{1}{Re}\frac{\partial^2\overline{u}}{\partial y^2},\tag{7}$$

where the overbar indicates the average value of the corresponding plane for a constant y.

Integrating Eq. (7) from 0 to 1 in the y direction with the friction drag coefficient defined as $C_f = \tau_w/\left(\rho U_c^2/2\right)$, then

$$\Pi(t) = -\left.\frac{1}{Re}\frac{\partial\overline{u}}{\partial y}\right|_w = -\tau_w = -\frac{C_f}{2}.\tag{8}$$

Substituting Eq. (8) into Eq. (7), we have

$$\frac{C_f}{2}=\frac{\partial}{\partial y}\left(\overline{uv}-\frac{1}{Re}\frac{\partial\overline{u}}{\partial y}\right)+\frac{\partial\overline{u'}}{\partial t}.\tag{9}$$

With the triple integral $\int_0^1\int_0^y\int_0^y f(y)\mathrm{d}y\mathrm{d}y\mathrm{d}y$ of Eq. (9), one obtains

$$C_f=\frac{4}{Re}+6\int_0^1(1-y)\left(-\overline{u'v'}\right)\mathrm{d}y-3\int_0^1(1-y)^2\frac{\partial u'}{\partial t}\mathrm{d}y.\tag{10}$$

And for the steady turbulence

$$\frac{\partial\overline{u'}}{\partial t}=0.\tag{11}$$

Substituting Eq. (11) into Eq. (10), the friction drag coefficient is obtained

$$C_f=\frac{4}{Re}+6\int_0^1(1-y)\left(-\overline{u'v'}\right)\mathrm{d}y.\tag{12}$$

The equation indicates that the friction drag coefficient is composed of two parts for the steady turbulent channel flow. The first term is the laminar drag coefficient, which depends on Reynolds numbers. The second term is the y-weighted integration of $\overline{u'v'}$, which is the Reynolds stress due to the ejection and sweep in the turbulence.

Define

$$C_{f0}=\frac{4}{Re},\tag{13}$$

$$C_{f(y)}=6\int_0^y(1-y)\left(-\overline{u'v'}\right)\mathrm{d}y.\tag{14}$$

Taking the derivative of Eq. (14), the distribution of $C_{f(y)}$ with y is

$$C^y_{f(y)}=6(1-y)\left(-\overline{u'v'}\right).\tag{15}$$

Generally, we have

$$y\equiv\delta_v y^+,\tag{16}$$

where δ_v is the viscous lengthscale and y^+ is the wall units.

Substituting Eq. (16) into Eq. (15), we have

$$C^{y^+}_{f(y^+)}=6\left(1-\delta_v y^+\right)\left(-\overline{u'v'}\right).\tag{17}$$

The contribution of the Reynolds stress on the different locations in the wall-normal direction can be described in Eq. (17).

2.3. Program verification

For the sake of testing the code and algorithm, the turbulent channel flow without control for $Re = 4000$, 5000, 6000, and 7000 is compared with the result from Kim *et al.*[24] The result indicates that the mean velocity profiles for $Re = 4000$, 5000, 6000, and 7000 in the paper are coincident and correspond with those in Ref. [24] and the classic wall law.

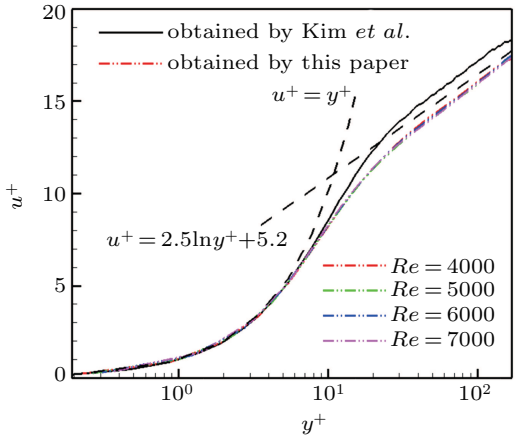


Fig. 2. Mean velocity profile of the turbulence without control.

3. Results and discussion

The induced flow field is a stable laminar flow field with the effect of electromagnetic force. The spanwise electromagnetic force introduced in the paper is defined by Eq. (4), which is independent of time. The spatial distribution of electromagnetic force with parameters $k_x = 3$, $A = 1.0$, and $\Delta = 0.02$, as a case, is shown in Fig. 3. The electromagnetic force can induce spanwise motion in the conductive fluid, and produce layers called Stokes layer near the wall. When the conductive fluid is affected by the electromagnetic force, as a case of the laminar flow field for $Re = 4000$, the spanwise velocity distribution of the induced laminar flow field is presented in Fig. 4, where the red and blue areas refer to the positive and negative values, respectively. As a result of the main flow along the positive direction of the x-axis, the distribution of the spanwise velocity is inclined significantly to the downstream, which is asymmetric but periodic with the electromagnetic force.

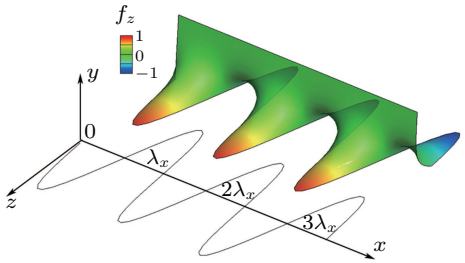


Fig. 3. The spatial distribution of electromagnetic force.

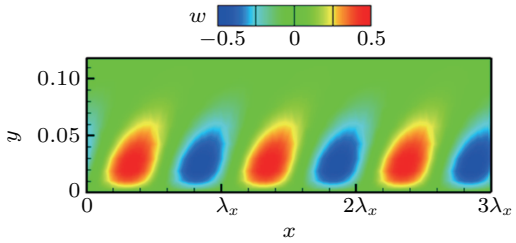


Fig. 4. The spanwise velocity distribution of the induced laminar flow field.

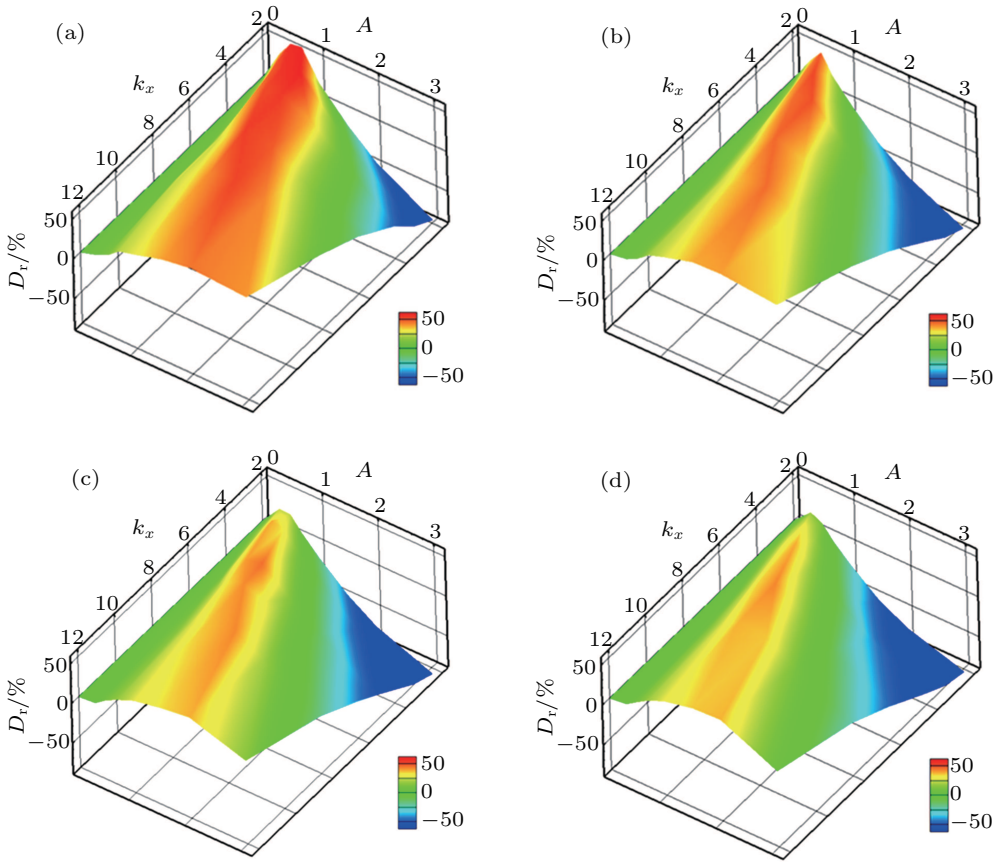


Fig. 5. The variations of drag reduction rate with amplitude and wave number for different Reynolds numbers: (a) $Re = 4000$, (b) $Re = 5000$, (c) $Re = 6000$, and (d) $Re = 7000$.

In the flow control, the rate of drag reduction is usually introduced to evaluate the control effect of electromagnetic force, which is defined as

$$D_r = (1 - < \tau_w > / < \tau_{wn} >) \times 100\%, \tag{18}$$

where $< \tau_w >$ and $< \tau_{wn} >$ are the average values of the wall shear stress with and without control, respectively. The variations of D_r with k_x and A are shown in Fig. 5, where figures 5(a), 5(b), 5(c), and 5(d) correspond to the cases of $Re = 4000$, 5000, 6000, and 7000, respectively. From the figures, the variations of D_r with the parameters of electromagnetic force have similar distributions for different Reynolds

numbers. At low wave numbers, the values of drag reduction rate vary dramatically with the amplitude (i.e., the absolute values of the reduction and increase in drag are large), whereas the values of that vary slowly at high wave numbers. Moreover, the maximum drag reduction can be obtained with the optimal parameter combination in each case of the four Reynolds numbers. The parameters of electromagnetic force correspond to the maximum drag reduction rate in Fig. 5, as shown in Table 1. From the table, the maximum drag reduction rate decreases as the Reynolds numbers increase, and the corresponding wave number of electromagnetic force increases, while the variation of the amplitude is around 1.0.

Table 1. The parameter combinations corresponding to the maximum drag reduction rate for different Reynolds numbers.

Reynolds number	Maximum drag reduction rate	Wave number	Amplitude
4000	58.9%	3	1.0
5000	49.4%	4	1.0
6000	45.2%	5	1.0
7000	42.4%	6	1.0

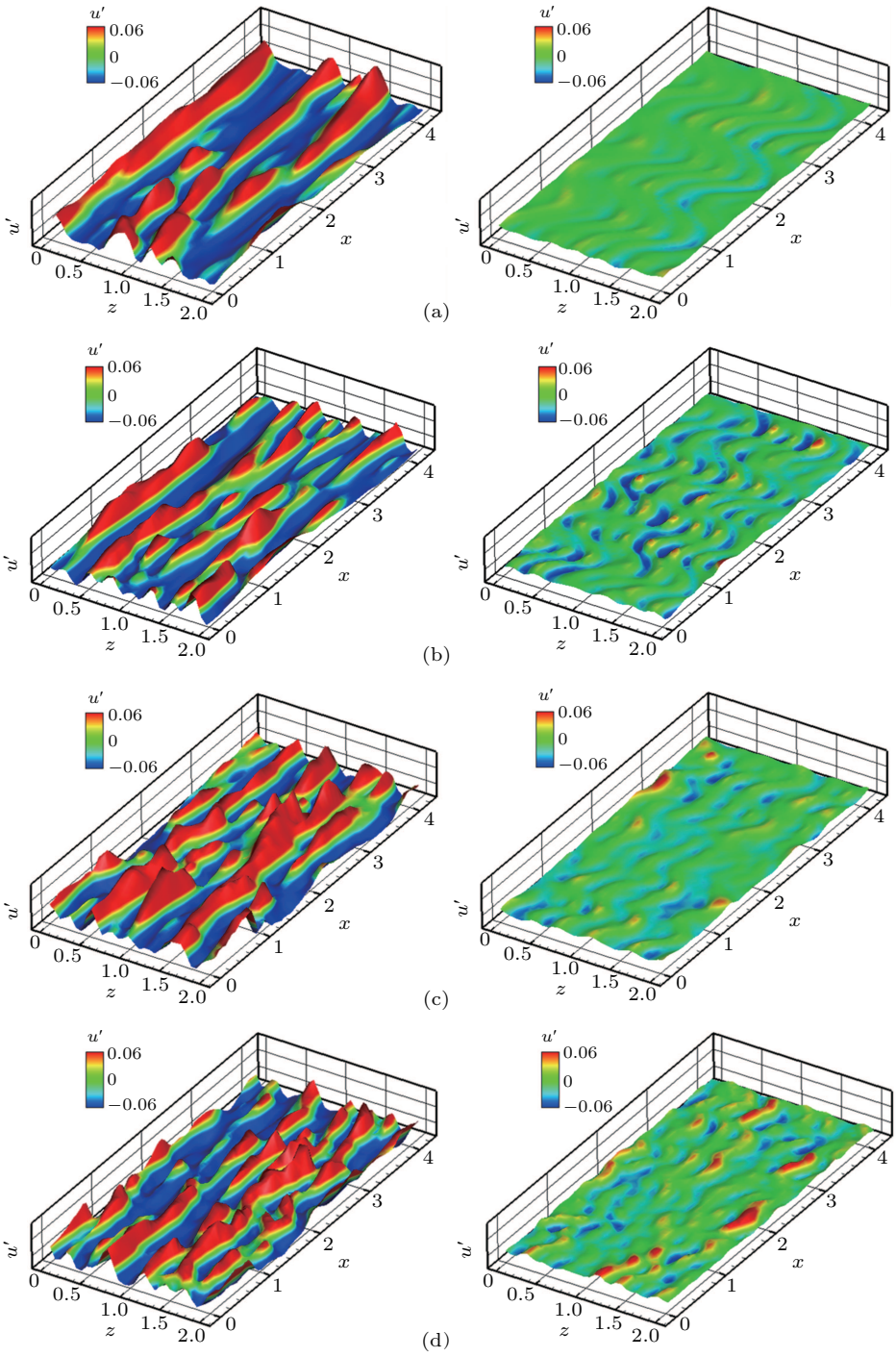


Fig. 6. The distribution of streaks at $y^+ = 5$ in the flow field before and after control with the optimal electromagnetic force: (a) $Re = 4000$, (b) $Re = 5000$, (c) $Re = 6000$, and (d) $Re = 7000$.

To find the reasons that the maximum drag reduction rate decreases with the increase of Reynolds number, it is necessary to study the in-depth mechanisms from the flow fields before and after control, respectively. The streaks are the basic elements of near wall turbulence coherent structures. Therefore, the distribution of streaks in the flow field at $y^+ = 5$ is first investigated, as shown in Fig. 6, where figures 6(a), 6(b), 6(c), and 6(d) represent the cases of $Re = 4000$, 5000, 6000, and 7000, respectively. The left figures indicate the distribution of streaks before control, and the right figures indicate the distribution of streaks after control with the electromagnetic force in Table 1, where red and blue represent high-speed and low-speed streaks, respectively. As shown in the left figures, high-speed and low-speed streaks are alternate with different lengths and curvatures in the flow field for $Re = 4000$. With the increase of Reynolds number, the strength of high-speed and low-speed streaks is enhanced, and the number of these streaks is increased. However, in the right figures, the strength of high-speed and low-speed streaks controlled by electromagnetic force at $Re = 4000$ is decreased significantly in the flow field. The distributions of these streaks are alternate along the spanwise direction with the well-organized characters. In particular, the periods of these streaks along the streamwise direction are the same as that of the electromagnetic force. Moreover, the distributions of high-speed and low-speed streaks are similar to the increase of Reynolds number, while the strength of these streaks is enhanced and the regularity of the streaks is gradually weakened. The control effects of the optimal electromagnetic force decay with the increase of Reynolds number.

The variations of fluctuating velocities (i.e., u', v', and w') can be further investigated and their values can be obtained from the value on each grid point before and after control. Therefore, with the coordinate axes u', v', and w', the discrete distributions of u', v', and w' for $y^+ = 5$ are obtained from values of fluctuating velocities on these locations ($y^+ = 5$), as shown in Fig. 7. Here, black and red discrete points represent the distributions of fluctuating velocities before and after control, respectively. Figures 7(a), 7(b), 7(c), and 7(d) correspond to the results of $Re = 4000$, 5000, 6000, and 7000, respectively. For the case of $Re = 4000$ before control, the distributions of u', v', and w' are dispersed. After control, the distributions of u' and v' converge to the origin, especially for u', which means that their absolute values are decreased. However, the absolute value of w' is increased dramatically and the distribution region of w' is enlarged with the effect of the

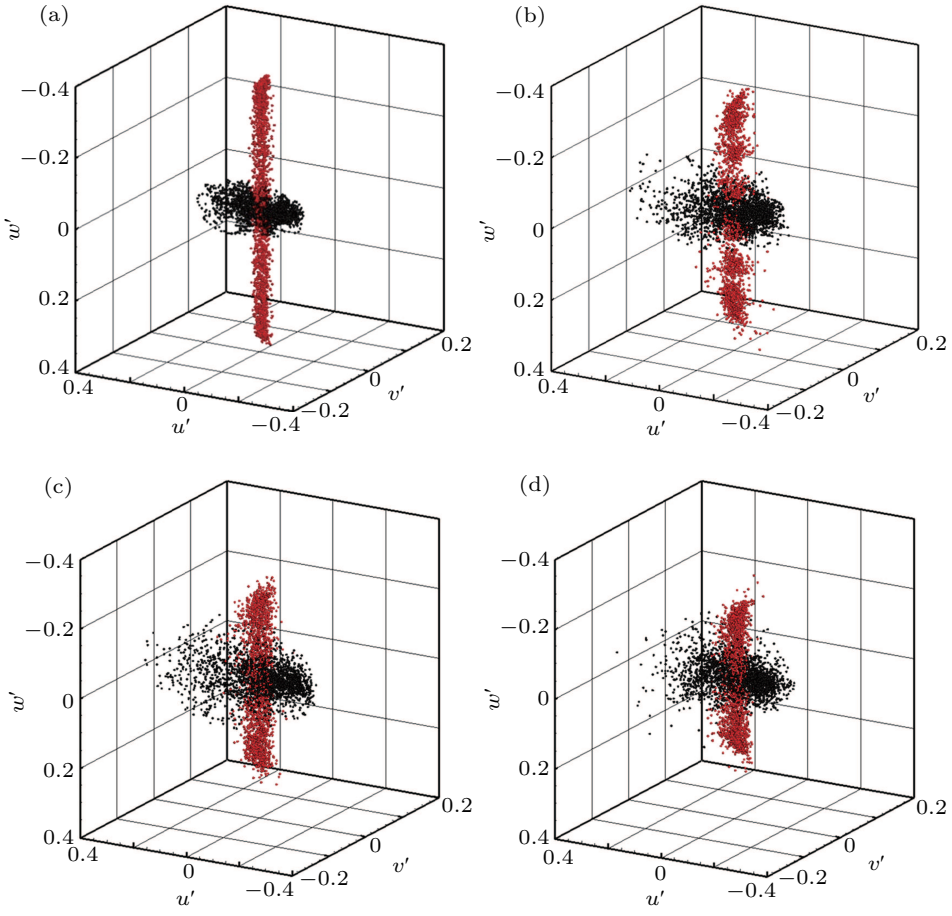


Fig. 7. The discrete distribution of fluctuating velocities at $y^+ = 5$ before and after control with the optimal electromagnetic force: (a) $Re = 4000$, (b) $Re = 5000$, (c) $Re = 6000$, and (d) $Re = 7000$.

spanwise electromagnetic force. These variations eventually lead to the straight cylindrical distribution of fluctuating velocities after control as red discrete points in Fig. 7(a). From Eq. (12), drag is a function with respect to u' and v' rather than w'. Therefore, the increase of w' does not lead to the increase of drag, while the decrease of u' and v' leads to the decrease of drag. Moreover, the distribution regions of the three fluctuating velocities gradually increase with the increase of Reynolds number, as shown in Figs. 7(b), 7(c), and 7(d), which means that some values of the fluctuating velocities increase. After control, the central tendency of the fluctuating velocities is weakened, which means that the control effect of the optimal electromagnetic force is weakened.

The Reynolds stresses depend on the product of u' and

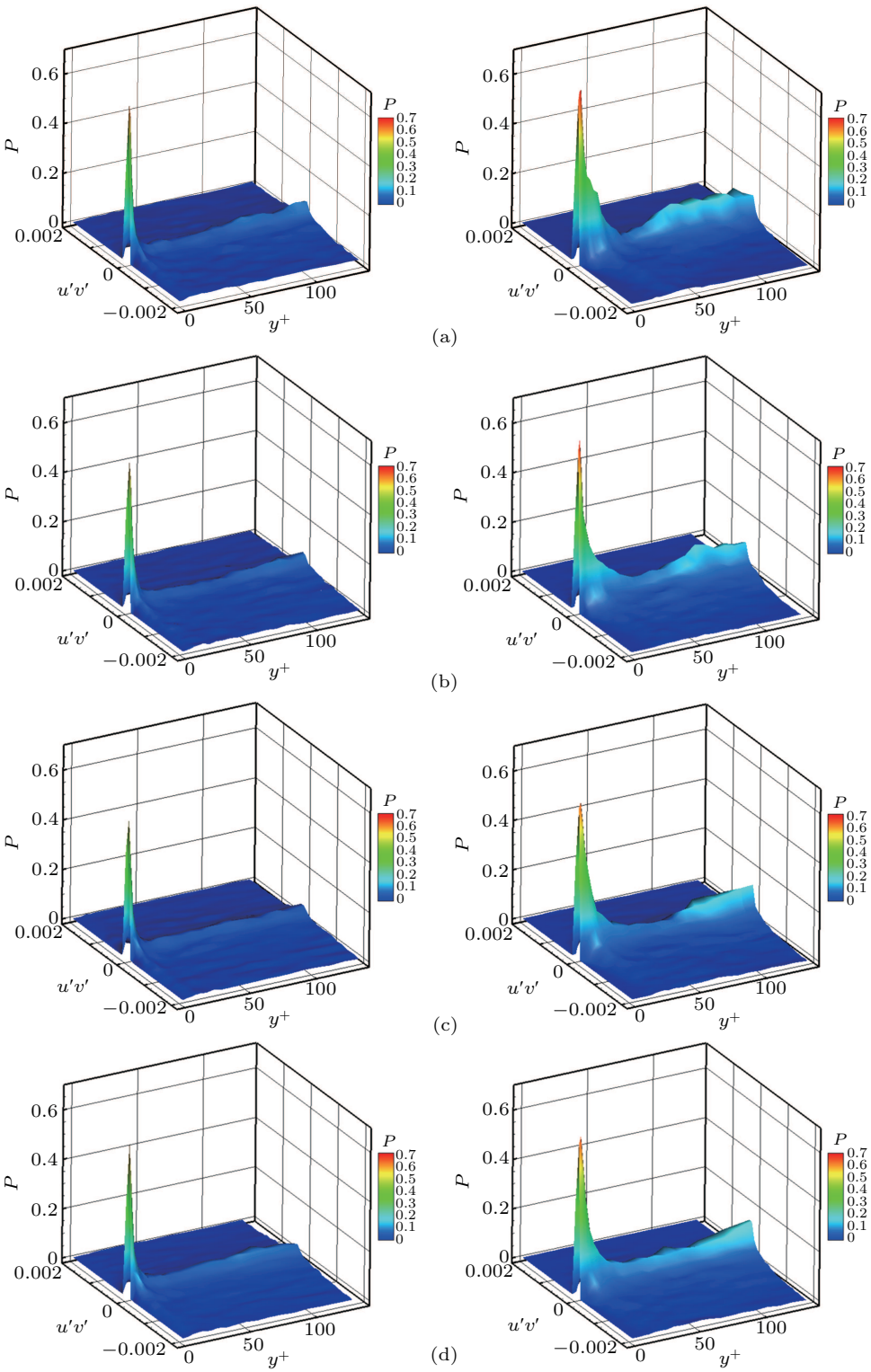


Fig. 8. The variation of probability distributions of $u'v'$ with y^+ before and after controlling the optimal electromagnetic force: (a) $Re = 4000$, (b) $Re = 5000$, (c) $Re = 6000$, and (d) $Re = 7000$.

v' rather than w'. Therefore, the variations of the product can be described by the probability distributions of $u'v'$ with y^+, where the left and right figures in Fig. 8 respectively represent the cases before and after control, and figures 8(a), 8(b), 8(c), and 8(d) correspond to the cases of $Re = 4000$, 5000, 6000, and 7000, respectively. P is the value of probability at a constant y^+, which is defined as

$$P\left(c_1 \leqslant u'v' \leqslant c_2\right) = \frac{N_{c_1c_2}}{N_x \times N_z}. \tag{19}$$

Here, $[c_1, c_2]$ is a subinterval of $[-0.002, 0.002]$ which is the range of the value of $u'v'$. $N_{c_1c_2}$ is the number of the value of $u'v'$ distributed in $[c_1, c_2]$. N_x and N_z are the numbers of grid points in the x and z directions, respectively. Red and blue areas represent the large and small values, respectively. From the case before control in Fig. 8(a), the distribution of $u'v'$ almost converges to $u'v' = 0$, and the peak value of P is large due to the flow dominated by the effect of viscosity in the area $y^+ < 5$. With the increase of y^+, the influence of turbulent fluctuation dramatically strengthens and exceeds the effect of viscosity, which leads to the increase of the value $u'v'$ in some regions. Therefore, the distribution of $u'v'$ is more homogeneous and the peak value of P is decreased rapidly. However, with the optimal electromagnetic force, the distribution of $u'v'$ is significantly close to $u'v' = 0$ in near-wall regions ($y^+ \leq 30$), which indicates that the values of $u'v'$ have been suppressed effectively. In the region $y^+ > 30$, the central tendency of $u'v'$ distribution is weakened, which means the control effect is weakened, because the electromagnetic force decays rapidly with the increase of y according to Eq. (4). As the Reynolds number increases, similar variations are obtained in Figs. 8(b), 8(c), and 8(d). However, the central tendency of $u'v'$ distribution is weakened (particularly in the regions $y^+ \leq 30$), which means that the control effects of the optimal electromagnetic force decrease with the increase of Reynolds number.

The Reynolds stresses $\overline{u'v'}$ can be obtained from the mean value of $u'v'$. According to Eq. (17), the turbulent drag coefficient $C^{y^+}_{f(y^+)}$ depends on the y^+-weighted integration of $\overline{u'v'}$, which has a larger weight near the wall in the component of turbulent drag. The distributions of $C^{y^+}_{f(y^+)}$ and $\overline{u'v'}$ before and after control by the optimal electromagnetic force for different Reynolds numbers are shown in Fig. 9, where figures 9(a), 9(b), 9(c), and 9(d) correspond to the computational results for $Re = 4000$, 5000, 6000, and 7000, respectively. From the case of $Re = 4000$ in Fig. 9(a), the absolute value of $\overline{u'v'}$ before control increases rapidly at first then decreases slowly with the increase of y^+, and $C^{y^+}_{f(y^+)}$ has similar variations. After control, the absolute value of $\overline{u'v'}$ decreases significantly, especially near the wall. The reason is that the values of $u'v'$ have been suppressed effectively with the effect of the optimal electromagnetic force, particularly in the region of $y^+ \leq 30$, as shown in Fig. 8. Therefore, $C^{y^+}_{f(y^+)}$ decreases with the decrease of the absolute value of $\overline{u'v'}$ based on Eq. (17). Moreover,

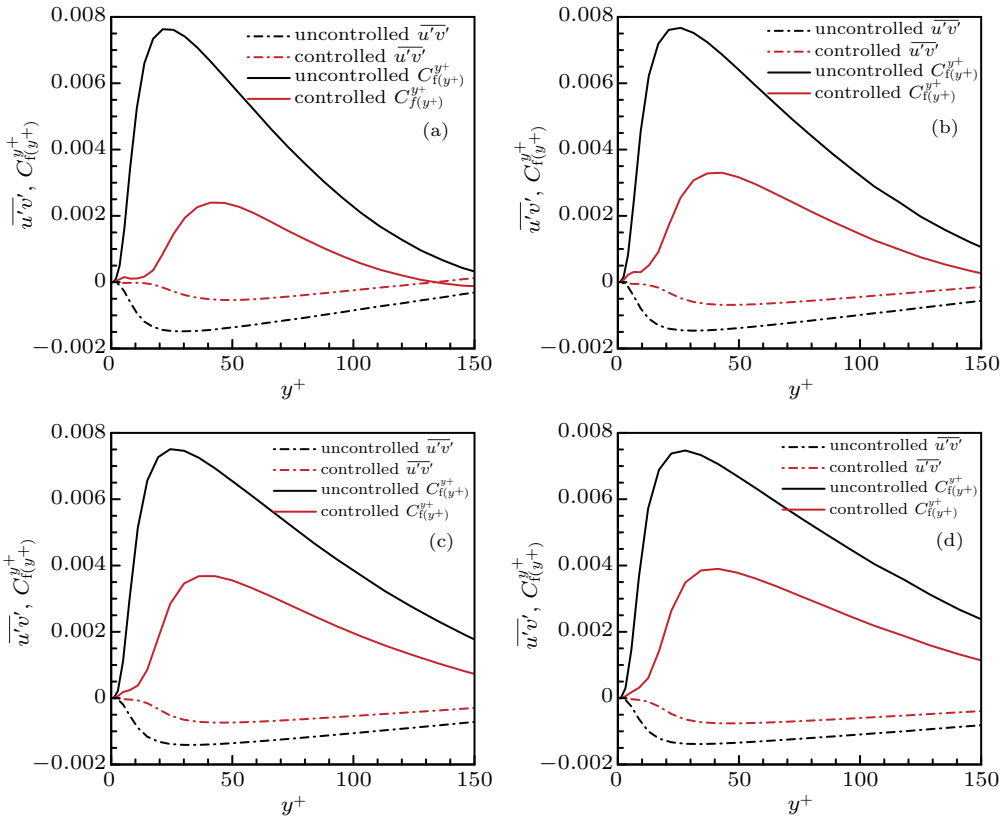


Fig. 9. The distribution of turbulent drag and Reynolds stress before and after control by the optimal electromagnetic force with y^+ for different Reynolds numbers: (a) $Re = 4000$, (b) $Re = 5000$, (c) $Re = 6000$, and (d) $Re = 7000$.

the suppression effect of the optimal electromagnetic force for $\overline{u'v'}$ is weakened with the increase of Reynolds number, as shown in Figs. 9(b), 9(c), and 9(d), due to the weakening effect of the central tendency of $u'v'$ distribution in Figs. 8(b), 8(c), and 8(d). Therefore, the absolute values of $\overline{u'v'}$ increase, which leads to the increase of $C^{y^+}_{f(y^+)}$ and indicates the weakening effect of drag reduction with the increase of Re in Fig. 9.

4. Conclusion

The relations on fluctuating velocities and the friction drag coefficient with the spanwise space-dependent electromagnetic force in turbulent channel flow and the mechanism of drag reduction are investigated with DNS for different Reynolds numbers. The results show that the maximum drag reductions are obtained with an optimal combination of parameters for each case of different Reynolds numbers. With the application of the optimal electromagnetic force, u' and v' (i.e., the fluctuating velocities along the streamwise and normal directions) are suppressed, while w' (i.e., the fluctuating velocity along the spanwise direction) is enhanced dramatically due to the spanwise electromagnetic force. However, the values of Reynolds stress depend on u' and v' rather than w'. Therefore, the distributions of u' and v' converge to the origin point, and the distributions of the product $u'v'$ also converge to $u'v' = 0$, which further leads to the decrease of Reynolds stress and drag reduction. Moreover, the control effect of the optimal electromagnetic force for the three fluctuating velocities gradually decays with the increase of Reynolds numbers, resulting in the weakening effects of central tendency for $u'v'$. Finally, the maximum drag reduction decreases due to the decay of control effect for Reynolds stress with the increase of Reynolds number.

References

[1] Wang L, Xia Z X, Luo Z B, Zhou Y and Zhang Y 2014 *Acta Phys. Sin.* **63** 194702 (in Chinese)
[2] Cao Y F, Gu Y S, Cheng K M, Xiao Z Y, Chen Z B and He K F 2015 *Acta Aeronaut. Astronaut. Sin.* **36** 757 (in Chinese)
[3] Meng X S, Long Y X, Wang J L, Liu F and Luo S J 2018 *Phys. Fluids* **30** 024101
[4] Zhang Z B, Wu Y, Jia M, Song H M, Sun Z Z and Li Y H 2017 *Chin. Phys. B* **26** 065204
[5] Liu M K, Zhang H, Fan B C, Han Y and Gui M Y 2016 *Acta Phys. Sin.* **65** 244702 (in Chinese)
[6] Auteri F, Baron A, Belan M, Campanardi G and Quadrio M 2010 *Phys. Fluids* **22** 115103
[7] Lim J, Choi H and Kim J 1998 *Phys. Fluids* **10** 1997
[8] Jiménez J and Pinelli A 1999 *J. Fluid Mech.* **389** 335
[9] Satake S I and Kasagi N 1996 *Int. J. Heat Fluid Flow* **17** 343
[10] Du Y and Karniadakis G E 2000 *Science* **288** 1230
[11] Du Y, Symeonidis V and Karniadakis G E 2002 *J. Fluid Mech.* **457** 1
[12] Lee C and Kim J 2002 *Phys. Fluids* **14** 2523
[13] Yin J F, You Y X, Li W and Hu T Q 2014 *Acta Phys. Sin.* **63** 044701 (in Chinese)
[14] Quadrio M, Ricco P and Viotti C 2009 *J. Fluid Mech.* **627** 161
[15] Viotti C, Quadrio M and Luchini P 2009 *Phys. Fluids* **21** 115109
[16] Moubarak L M and Antar G Y 2012 *Exp. Fluids* **53** 1627
[17] Habchi C and Antar G 2016 *Phys. Fluids* **28** 055102
[18] Ostillamónico R and Lee A A 2017 *Far. Disc.* **199** 159
[19] Altıntaş A and Davidson L 2017 *Acta. Mech.* **228** 1269
[20] Huang L P, Fan B C and Dong G 2010 *Phys. Fluids* **22** 015103
[21] Huang L P, Choi K S, Fan B C and Chen Y H 2014 *Sci. Chin.-Phys. Mech. Astron.* **57** 2133
[22] Han Y, Zhang H, Fan B C, Li J, Jiang D W and Zhao Z J 2017 *Chin. Phys. B* **26** 084704
[23] Fukagata K, Iwamoto K and Kasagi N 2002 *Phys. Fluids* **14** L73
[24] Kim J, Moin P and Moser R 1987 *J. Fluid Mech.* **177** 133